

# Local wind speed forecasting at short time horizons relying on both Numerical Weather Prediction and observations from surrounding stations

ROBERTA BAGGIO,<sup>a</sup> KILLIAN PUJOL,<sup>b</sup> FLORIAN PANTILLON,<sup>b</sup> DOMINIQUE LAMBERT,<sup>b</sup> JEAN-BAPTISTE FILIPPI,<sup>a</sup>  
JEAN-FRANÇOIS MUZY,<sup>a</sup>

<sup>a</sup> *Laboratoire Sciences Pour L'Environnement (SPE), UMR 8134, CNRS, Université de Corse, Campus Grimaldi, 20250 Corte, France*

<sup>b</sup> *Laboratoire d'Aérodynamique (LAERO), Université de Toulouse, CNRS, UTII, IRD*

**ABSTRACT:** This study presents a hybrid neural network model for short-term (1-6 hours ahead) surface wind speed forecasting, combining Numerical Weather Prediction (NWP) with observational data from ground weather stations. It relies on the MeteoNet dataset, which includes data from global (ARPEGE) and regional (AROME) NWP models of the French weather service and meteorological observations from ground stations in the French Mediterranean. The proposed neural network architecture integrates recent past station observations (over last few hours) and AROME and ARPEGE predictions on a small subgrid around the target location. The model is designed to provide both deterministic and probabilistic forecasts, with the latter predicting the parameters of a suitable probability distribution that notably allows us to capture extreme wind events. Our results demonstrate that the hybrid model significantly outperforms baseline methods, including raw NWP predictions, persistence models, and linear regression, across all forecast horizons. For instance, the model reduces RMSE by up to 30% compared to AROME predictions. Probabilistic forecasting further enhances performance, particularly for extreme quantiles, by estimating conditional quantiles rather than relying solely on the conditional mean. Fine-tuning the model for specific stations, such as those in the Mediterranean island of Corsica, further improves forecasting accuracy. Our study highlights the importance of integrating multiple data sources and probabilistic approaches to improve short-term wind speed forecasting. It defines an effective approach, even in a complex terrain like Corsica where localized wind variations are significant.

## 1. Introduction

Wind speed forecasting is an important issue that concerns many applications, from public safety to renewable energy production. In the energy sector, where the production of wind farms is inherently variable, accurate wind forecasts over short-term horizons (few hours) are crucial for enabling grid operators and wind farm managers to balance supply and demand, plan operations effectively, and mitigate risks (Shaw et al. 2019). Similarly, reliable short-term wind speed forecasts are essential for protecting public welfare by providing critical information for aviation, shipping, and other weather-sensitive human activities, especially in the case of severe wind episodes (Pinto et al. 2019). However, the turbulent and intermittent nature of wind, combined with rapid variations in local conditions, makes short-term wind prediction a highly complex task (Pantillon et al. 2020).

Traditional weather forecasting relies heavily on Numerical Weather Prediction (NWP) models, which simulate atmospheric dynamics based on physical principles and use initial conditions derived from observational data.

National weather services usually combine NWP models at the global and regional scales to produce forecasts. For instance, Météo France uses the ARPEGE and AROME models: ARPEGE (Courtier et al. 1994), a global model with a refined resolution of about 5 km over Europe and France, provides broader-scale forecasts up to 5 days ahead but is limited in its ability to capture local phenomena; AROME (Seity et al. 2011) is a high-resolution mesoscale

model downscaled from ARPEGE, specifically designed for shorter-range forecasts up to 2 days ahead and with a horizontal resolution of 1.3 km, which makes it effective in resolving weather phenomena at smaller scales and deep convection in particular. Despite the considerable progress made in recent decades (Bauer et al. 2015), NWP models are computationally intensive and often struggle to provide accurate predictions at fine spatial and temporal scales. Designed primarily for meso to synoptic scales  $O(10-1000\text{ km})$ , NWP models are less effective in capturing localized variations and rapidly evolving phenomena such as wind gusts (Pantillon et al. 2018) or local convective episodes (Yano et al. 2018). Moreover, since the atmosphere is a chaotic system, it is desirable to provide forecasts with an estimate of the associated uncertainty, that is, to make probabilistic predictions. For this reason, operational centers produce ensemble forecasts, which consist of multiple runs of the same NWP, obtained using stochastically perturbed initial conditions and physical equations, or by aggregating results from different models (or both; Swinbank et al. 2016), a fact that makes NWP forecasts even more costly.

To address those limitations of NWP models for wind speed “nowcasting” (namely, forecasting at horizons up to few hours) a range of statistical, Machine Learning (ML) and Deep Learning (DL) methods has emerged. These methods mainly rely on statistical inference or time-series model based approaches that use historical data and focus on past observed patterns to forecast future observations (see e.g., Tascikaraoglu and Uzunoglu (2014) and references therein). Some of these techniques involve the devel-

---

Corresponding author: J.F. Muzy, muzy@univ-corse.fr

opment of specific stochastic models in order to account for observed fluctuations, particularly within the realm of time series analysis (Baïle et al. 2011). Most of the recent approaches leverage more advanced ML and DL techniques. In particular, artificial Neural Networks (NN) have proven to be very efficient in capturing the nonlinear dependencies that define wind dynamics. Numerous neural network models with many different architectures have been proposed so far. The most commonly used models are Recurrent Neural Networks, temporal or spatial Convolutional Networks, Graph Convolutional Networks or transformer based models. A comprehensive overview of this rapidly evolving field can be found in numerous review papers (see e.g., Hanifi et al. (2020); Wang et al. (2021)).

Besides pure NWP or pure statistical approaches, hybrid methods that combine the two have been experimented in order to produce better predictions, especially at short-term (Huang et al. 2012). Hybrid models, as the name suggests, aim to take advantage of the strengths of both NWP and statistical methods. These models may incorporate NWP output as predictors within statistical frameworks, such as time series models or ML approaches (like e.g., NN models). In these cases, one expects that the NWP forecasts provide valuable information about large-scale atmospheric conditions, while processing observational data allows one to account for local effects, model biases, and unresolved sub-grid processes to improve wind speed or wind power nowcasting (Hoolohan et al. 2018; Brabec et al. 2021; Donadio et al. 2021; He et al. 2022). Let us notice that such approaches are very close to the so-called statistical post-processing of NWP forecasts (Vannitsem et al. 2021). Indeed, it is well known that direct forecasting from NWP, regardless of whether it is global or regional, often exhibits systematic biases and limitations, particularly at the local scale and close to the surface for variables like wind speed (Zamo et al. 2016). These errors stem from factors such as insufficient model resolution, incomplete representation of physical processes, and inaccuracies in initial conditions. For that reason, operational centers consider various post-processing methods in order to remove those biases and improve prediction. The most commonly used method is the “Model Output Statistics” (MOS) which consists of regressing observed data from raw NWP outputs. This framework has been extended to probabilistic forecasting with the “Ensemble Model Output Statistic” (EMOS) that was designed to handle ensemble predictions (Gneiting et al. 2005). More elaborated statistical methods, that can capture non-linear, complex relationships between NWP outputs and observed weather variables like Kalman filtering (Pelosi et al. 2017), random forests (Zamo et al. 2016) or NN models (Rasp and Lerch 2018; Veldkamp et al. 2021) have been proposed more recently. Consequently, advancements in NWP post-processing methods and hybrid model approaches have made them increasingly

difficult to distinguish, as both allow for improved short-term forecasting accuracy by integrating NWP with local observational data.

This study contributes to the development of hybrid statistical methods for reliable nowcasting of surface wind speed. It leverages the MeteoNet database, an open-access resource provided by Météo France, which includes both NWP and observational data (Larvor et al. 2020). MeteoNet covers two regions of France—the Southeast and Northwest—and provides essential meteorological variables at hourly and sub-hourly temporal resolutions, making it well-suited for training and validating ML models for short-term, location-specific forecasts. We focus on the French Mediterranean region, particularly Corsica, a French Mediterranean island ( $80 \times 180$  km) characterized by complex mountainous terrain and frequent high-impact meteorological events such as windstorms, heavy rain-fall, thunderstorms and Saharan dust incursions (Schefknecht et al. 2017; Coquillat et al. 2019; Lfarh et al. 2023). The Mediterranean region is also a recognized climate change hotspot, motivating various research initiatives (e.g., Drobinski et al. 2014; Hatzaki et al. 2023). We introduce a NN model to enhance short-term wind speed forecasting in this geographically complex setting. Our model integrates NWP data from both global (ARPEGE) and regional (AROME) models with station observations to generate deterministic and probabilistic forecasts for lead times of one to six hours at any given selected station. By combining the strengths of physically based NWP models and data-driven ML techniques, our proposed framework aims at capturing both large-scale weather patterns and localized wind variations in order to improve forecasting accuracy and adaptability to site-specific conditions. Our framework is designed to support operational needs in the wind energy sector, providing actionable insights for planning, risk mitigation, and decision-making.

Let us end this introductory section by mentioning that a similar approach, utilizing the same dataset, was recently proposed by Marcille et al. (2024) in order to forecast wind speed at offshore locations where observational data is unavailable.

The paper is organized as follows. In Section 2 we describe the MeteoNet dataset used in this work. Section 3 is devoted to the description of the forecasting task we focus on and of various models which performance are compared. We notably introduce the  $\mathcal{M}$  and  $\mathcal{M}'$  models that leverage both NWP and station MeteoNet data for producing respectively deterministic and probabilistic short-term surface wind speed forecasting. All the results are provided in Section 4. Subsection 4-a presents a comparative performance analysis of  $\mathcal{M}$  and  $\mathcal{M}'$  against various baselines for all considered stations, while 4-b focuses on the results of versions of the model specifically fine-tuned for sites in Corsica. Section 5 summarizes our findings and proposes various prospects for future research.

## 2. Data

### a. The MeteoNet database

The results presented in this article are based on the MeteoNet database, which is a comprehensive and freely available meteorological dataset published by Météo France, the French national meteorological service (Larvor et al. 2020). It has been specifically designed to support research and development in meteorology, climatology, and machine learning applications. The MeteoNet database contains high-resolution meteorological data over, respectively, the Northwest and Southeast quarters of the France territory covering the period from 01-01-2016 to 12-31-2018. It includes observations from ground-based weather stations, gridded forecasts from NWP models, and auxiliary geospatial information.

In this work, we will consider exclusively the Southeast data, influenced mostly by a Mediterranean climate with, as mentioned in the introduction, a special focus on sites spread all over Corsica. Observation data are provided by the Météo France ground station network, with a large number of stations (278 stations with a fraction of available data above a given threshold). The position of each of these stations is shown in Fig. 1(a). They provide, at a time resolution of 6 min, times records of different weather variables as notably 10 m wind speed and direction and 2 m air temperature. In this study, we also use the forecasts data from Météo France operational NWP models ARPEGE and AROME included in the MeteoNet database with 0.1° and 0.025° horizontal resolutions, respectively. A single run is provided for each day, the one beginning at 00 UTC that spans the forecast ranges from 00 to 24 UTC, with a time step of 1 h for the AROME data and 1 h or 3 h for the ARPEGE data, depending on the time horizon. AROME data are composed of different surface fields (notably 10 m wind speed, 2 m temperature, relative humidity and mean-sea-level pressure) whereas ARPEGE provides predictions of various fields (like horizontal wind speed components or temperature) at 7 different isobar levels spanning the low to mid troposphere and at 7 different heights in the lower troposphere for the pressure variable. The precise way we use a subset of these data in our model is described in Sec. 3.

### b. Wind speed station data in Corsica

Some of our results detailed in the following specifically focus on ground stations in Corsica. These stations correspond to the subset of locations represented in Fig. 1(b).

For comparison purpose, we also utilize a specific dataset of wind speed and direction time series previously used in Baggio and Muzy (2024). This dataset comprises hourly wind speed measurements recorded by Météo France at various locations across Corsica from January 1,

2011, to December 31, 2020. In the following, we focus on four specific sites—Ajaccio, Lucciana, Renno, and Figari—to compare the proposed approach with previous machine learning methods, such as the one introduced in Baïle and Muzy (2023), which relies exclusively on past observed data from the target station and its 15 closest neighboring stations. These four selected sites together with their neighboring stations have a low proportion of missing data, with less than 15% of the total possible data points unavailable. For this analysis, the period from January 1, 2011, to December 31, 2015, is used as the training sample, while the comparison is performed on the validation and test subsets from the MeteoNet 2016–2018 period.

## 3. Forecasting task and models

Our goal in this paper is to propose a model that provides wind speed forecasts at some single site over short term lead time of few hours. In this section, we set the main notations and describe this specific prediction goal in mathematical terms. We then introduce the main model designed to tackle this problem, along with alternative baseline models used for comparison.

### a. Prediction at multiple horizons

Let  $V_{d,t}^s$  be the surface wind velocity (in  $m s^{-1}$ ) at time  $t$  of day  $d$  at a given fixed location  $s$ . In all our experiments we consider the hourly frequency and thus, for a given day  $d$ ,  $t$  is expressed in hours. The upper character  $s$  can represent the longitude/latitude coordinates of the target location or simply the site name. Notice that  $V_{d,t}^s$  is directly recorded if  $s$  corresponds to a site where a ground station is installed. Let  $h_1 < h_2 < \dots < h_H$  be a fixed set of  $H$  increasing horizon values with  $H \geq 1$ . For the sake of simplicity and to avoid handling horizons too far away from NWP run initial time, we restrict ourselves to the set of horizon times  $h \in \{1, 2, 3, 4, 5, 6\}$  hours. This corresponds to  $H = 6$  with  $\{h_i = i\}_{i=1, \dots, 6}$  in the previous notations.

We denote by  $\mathbf{V}_{d,t+h}^s$  the  $H$ -dimensional vector of future velocities at multiple horizons:

$$\mathbf{V}_{d,t+h}^s = \begin{pmatrix} V_{d,t+h_1}^s \\ V_{d,t+h_2}^s \\ \vdots \\ V_{d,t+h_H}^s \end{pmatrix}.$$

Let us notice that the horizon time  $h$  can be also called forecast horizon or simply the horizon. In the literature  $h$  is also often referred to as the lead time (e.g. in Marcille et al. (2024)). The time  $t$  of the day when the prediction is performed will be called the initial time. The objective of all models discussed below is, for any given station  $s$ , any day  $d$  and initial time  $t$ , to provide the “best” prediction of upcoming velocity vector  $\mathbf{V}_{d,t+h}^s$ .

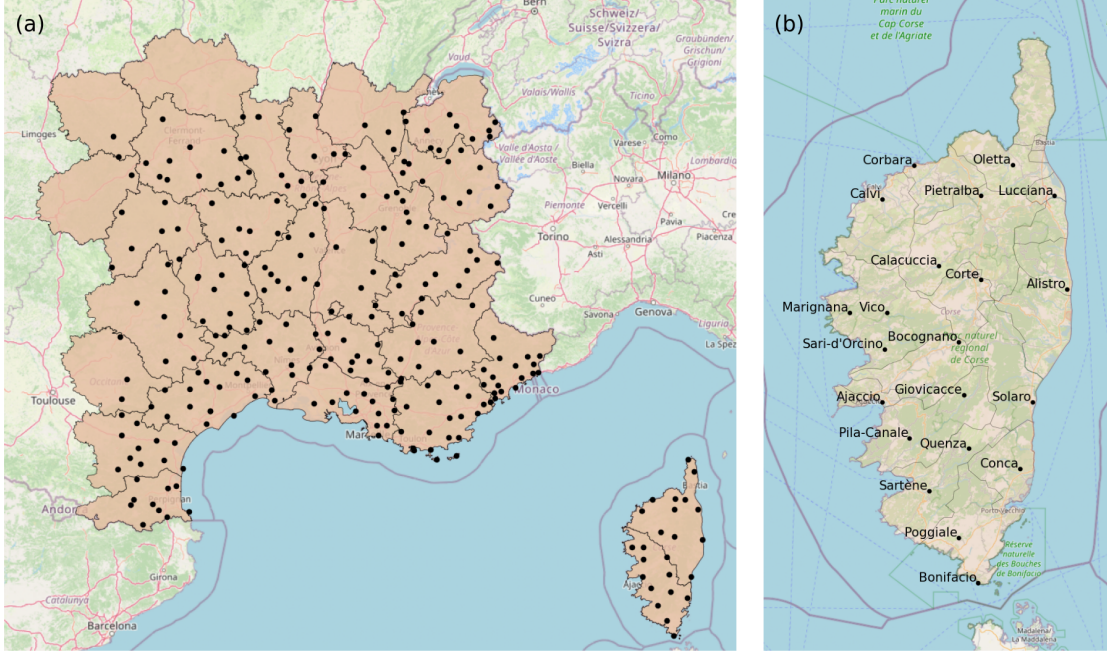


FIG. 1. (a) Geographical extent of the MeteoNet Southeast database, with the 278 ground station localizations (●). (b) Location and names of the 21 target ground stations in Corsica.

It is important to realize that, since in the MeteoNet dataset we only have access to NWP models initialized at 00 UTC (hereafter referred to as the *initialization time*), for a given initial time  $t$  and forecast horizon  $h$ , their predictions correspond to an *effective horizon* of  $t+h$ , which places them at a disadvantage. The experiment we conduct does not aim to compare NWPs in general—since these may be re-initialized multiple times per day—but rather those specifically from the 00 UTC run. For obvious reasons, we choose to compare results at a fixed forecast horizon  $h$ . Indeed, from an operational perspective, for any given initial  $t$  time within the day, this is the most relevant variable. Consequently, the conclusions of this study are based on the average performance over all  $t$  at fixed  $h$ , rather than at fixed  $t+h$ , thus encompassing weather phenomena that occur at different times of the day. In this framework, the performance of models that involve only AROME or ARPEGE predictions effectively integrates a range of *effective horizons*, which depends only marginally on  $h$ . As a result, we expect NWP-based results to exhibit very limited dependence on  $h$ .

The prediction vector will be denoted as  $\widehat{\mathbf{V}}_{d,t+h}^s$ . In general, at each day  $d$  and time  $t$ , the “best” predictor corresponds to the one that minimizes the conditional Mean Squared Error (MSE):

$$\mathcal{E}_{d,t}^{mse} = \mathbb{E} \left( \left\| \mathbf{V}_{d,t+h}^s - \widehat{\mathbf{V}}_{d,t+h}^s \right\|^2 \middle| \mathcal{F}_{d,t} \right) \quad (1)$$

where  $\mathcal{F}_{d,t}$  represents all the “information” available at day  $d$ , time  $t$  and  $\|\mathbf{Z}\|^2$  is the squared euclidian norm of  $\mathbf{Z}$ , i.e., the sum of its squared components:  $\sum_{i=1}^H Z_i^2$ .  $\mathbb{E}(\cdot | \mathcal{F}_{d,t})$  stands for the mathematical expectation conditionally to  $\mathcal{F}_{d,t}$  meaning the expectation associated with some (unobservable) conditional probability law of future outcome of weather conditions at times  $t+h$  that could be, for instance, defined within a Bayesian approach.

It can be shown that the vector  $\mathbf{M}_{d,t+h}^s$  that minimizes  $\mathcal{E}_{d,t}^{mse}$  is simply *the conditional mean*:

$$\mathbf{M}_{d,t+h}^s = \mathbb{E} \left( \mathbf{V}_{t+h}^s \middle| \mathcal{F}_{d,t} \right).$$

In that respect, for any station  $s$ , at any time  $t$  and day  $d$ , minimizing the MSE is equivalent to building  $\widehat{\mathbf{V}}_{d,t+h}^s$  as the best approximation of the conditional expectation  $\mathbf{M}_{d,t+h}^s$  of the multi-horizon velocity vector  $\widehat{\mathbf{V}}_{d,t+h}^s$ .

In practice, at each day  $d$  and time  $t$ , one “encodes” the information  $\mathcal{F}_{d,t}$  available at site  $s$  within a large vector of observable “features”  $\mathbf{X}_{d,t}^s$ . A commonly used possibility is then to seek for a *model*  $\mathcal{M}(\mathbf{X}_{d,t}^s, \Theta)$  that directly outputs  $\widehat{\mathbf{V}}_{d,t+h}^s$ :

$$\widehat{\mathbf{V}}_{d,t+h}^s = \mathcal{M}(\mathbf{X}_{d,t}^s, \Theta) \quad (2)$$

where  $\Theta$  is a set of model parameters.

Another option is to operate within the framework of the so-called “probabilistic forecasting”. Instead of providing a direct estimation of the conditional mean, the model

provides  $\widehat{\rho}_{d,t+h}^s(\mathbf{V})$ , an estimation of the conditional law of  $\mathbf{V}_{d,t+h}^s$ . As explained below, this can be done by various approaches like e.g. a direct output of a set of quantiles values of  $\widehat{\rho}_{d,t+h}^s$  or within a parametric method. In that case, the conditional mean  $\widehat{\mathbf{V}}_{d,t+h}^s$  is obtained as follows:

$$\widehat{\rho}_{d,t+h}^s = \mathcal{M}(\mathbf{X}_{d,t}^s, \Theta), \quad (3)$$

$$\widehat{\mathbf{V}}_{d,t+h}^s = \int_{\mathbb{R}^H} \widehat{\rho}_{d,t+h}^s(\mathbf{V}) \cdot \mathbf{V} dV_1 \dots dV_H \quad (4)$$

In the following sections we introduce a specific model  $\mathcal{M}$  that is built using a neural network architecture and whose final layer is configured to match the context described by Eq. (2) and a similar model  $\mathcal{M}'$  such that the output layer corresponds to the framework of Eq. (3). We also consider some of its simple variants together with baseline models for comparison purpose.

### b. A neural network model designed to handle station data and NWP predictions

The objective of this study is to explore the hybridization of NWP and observations using a streamlined neural network model. Rather than developing a state-of-the-art model, we employ a straightforward architecture with standard convolutional and recurrent layers for spatial and temporal feature extraction (Goodfellow et al. 2016). Identifying advanced architectures and optimizing model performance is left for future research.

Our “hybrid” neural network model that integrates NWP short-term forecasts with local ground station data is designed to process 3 distinct sets of MeteoNet input data: stations data, AROME predictions, and ARPEGE predictions. It is illustrated in Fig. 2. One can see that the model is composed of 3 branches devoted to handle the different input features. These features, associated with each branch, are summarized in Table 1. Let us describe more precisely the input feature data associated with each of the 3 parts of the model for any given location, that is, for any site referenced as a “ground station” in MeteoNet dataset.

Let  $\mathbf{GS}_{d,t}^s$ ,  $\mathbf{AR}_{d,t}^s$  and  $\mathbf{AP}_{d,t}^s$  be the feature tensors built from respectively the ground station, AROME and ARPEGE data at some given day  $d$ , time  $t$  and corresponding to some given site  $s$ . The first one, associated with weather ground station data, is composed of 3 different variables: the wind speed data ( $u, v$  components) and surface temperature data. Other measures like pressure or humidity have drastically lower number of available data, so we chose to restrict ourselves to wind speed and temperature features. For each site, we also include these 3 variables measured at the 10 closest surrounding weather stations for which the data are also available. In that respect, at any given  $(d, t, s)$ , the number of station input

variables is  $N_C = 33$ . At a given current time  $t$ , we are considering not only the measures at  $t$  but also the measures obtained 6 hours in the past i.e. at times  $t-1, \dots, t-6$ . At this stage, it is worth noting that the MeteoNet dataset provides ground station observations at a sampling frequency of 6 minutes. However, our experiments have shown that increasing the time resolution does not lead to any significant improvement in forecasting performance within our model. Therefore, to maintain model simplicity and minimize the number of parameters, we restrict our analysis to data at an hourly scale. The number considered of time periods (past or present) is then  $N_H = 7$ , so that the overall  $\mathbf{GS}_{d,t}^s$  tensor shape is  $(7 \times 33)$ .

Among all AROME prediction data, we select wind eastward and northward components at 10 m, mean-sea-level pressure, 2 m temperature and relative humidity so that the number of input variables is  $N_C = 5$ . We keep only data around the considered ground station position, i.e., we consider the set of  $11 \times 11$  AROME grid points centered around the ground station, namely if  $i_0, j_0$  are the coordinates of the grid point closest to the target ground station  $s$ , then the considered AROME predictions are those within a spatial extent of  $\pm 0.125^\circ$  latitude/longitude around this grid point. Moreover, we keep all prediction horizons  $t+1, t+2, \dots, t+6$  so that  $N_H = 6$ . The shape of the tensors  $\mathbf{AR}_{d,t}^s$  is therefore  $6 \times 5 \times 11 \times 11$ . We note that, since AROME forecasts data are only available for  $0 \leq t \leq 24$ , available features are restricted by the choice of the largest horizon  $h_H$ . That is, for each day  $d$ , we take  $t$  to be the range  $t = 0, 1, \dots, 18$ .

The  $\mathbf{AP}_{d,t}^s$  tensor, which contains the data from the ARPEGE NWP model, is constructed along the same line: we keep only wind eastward and wind northward components together with temperature at all 7 isobar levels and we also consider the pressure levels at all 7 heights. As far as prediction horizons are concerned, we consider the same 6 next hours set of horizons as for AROME. When the horizon is not available, we consider the closest horizon multiple of 3 hours (indeed, ARPEGE predictions are not available on a regular time grid, as the time step varies from 1 hour in the morning to 3 hours in the afternoon). Concerning the grid size, we use all grid points within an interval  $\pm 0.2^\circ$  around the closest point to the station. Notice that this spatial extent is larger than former AROME one but, due to the lower resolution of ARPEGE, it corresponds to a smaller  $(5 \times 5)$  grid size. Accordingly, the ARPEGE input tensors have a shape  $6 \times 4 \times 7 \times 5 \times 5$ .

As represented in Fig. 2 by blue 3D boxes, the branches that process AROME data ( $\mathbf{AR}_{d,t}^s$ ) and ARPEGE data ( $\mathbf{AP}_{d,t}^s$ ) inputs begin with a time-distributed convolution which applies the same spatial (2D for AROME and 3D for ARPEGE) convolution operation independently to each time step in a sequence of inputs, treating each time step as a separate sample. This allows the model to extract spatial features along the temporal axis while maintaining

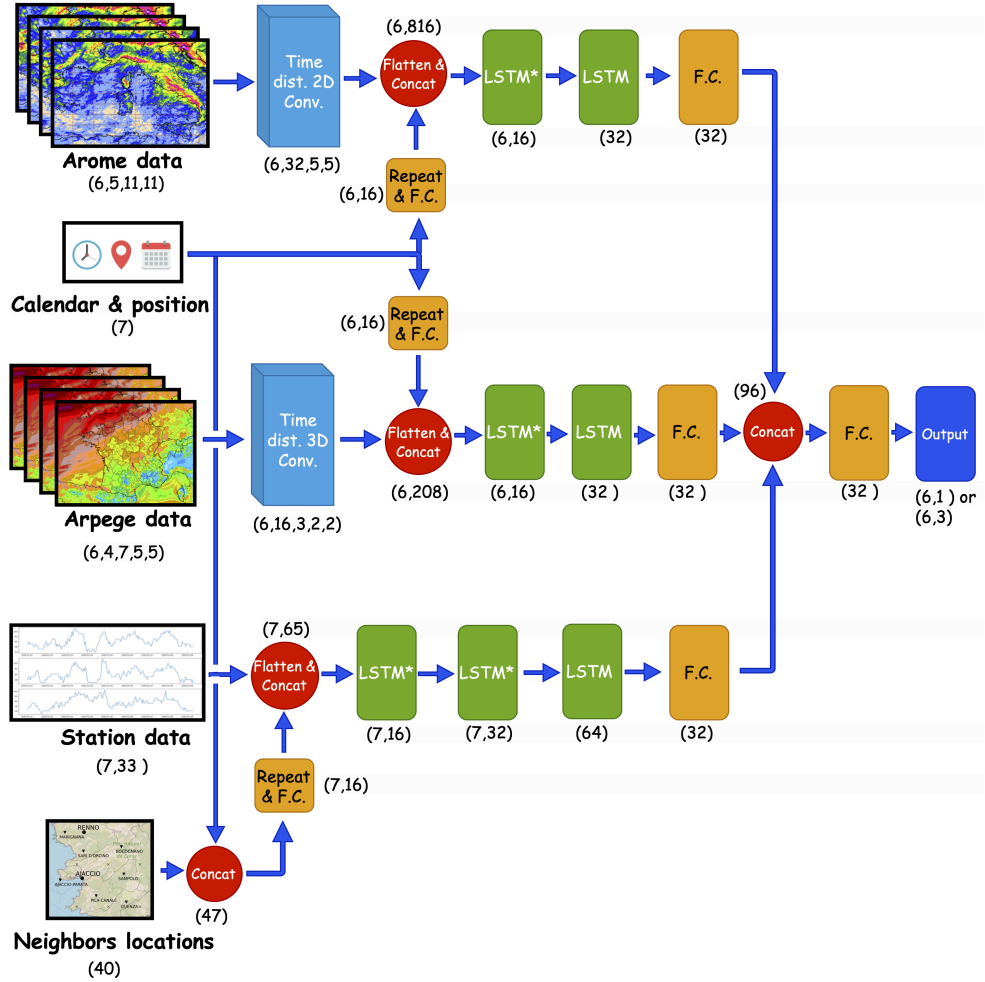


FIG. 2. Sketch of neural network architecture we use to handle station, AROME and ARPEGE data. Output shape is indicated under each layer. F.C. stands for “fully connected layer” and *LSTM\** means that the full sequence of outputs is returned and not only the final one.

TABLE 1. Summary of the MeteoNet input data used in the model  $M$

Input type	Space and time grids	Weather fields	Input shape
Stations	- Spatial grid: 11 locations (station + 10 neigh.) - Time grid: Current+6 past hourly values	- Wind $u,v$ (m/s) - Temp. (K) - 2 m Temp. (K)	$(7 \times 33)$
AROME	- Spatial grid : $(11 \times 11)$ - Time grid : All 6h ahead predictions	- 2 m Rel. humidity (%) - Wind $u,v$ (m/s) - Mean sea lev. Press. (Pa)	$(6 \times 5 \times 11 \times 11)$
ARPEGE	- Spatial grid : $(7 \times 5 \times 5)$ - Time grid : All 6 h ahead predictions	- Temp. (K) - Wind $u,v$ (m/s) - Pressure (Pa)	$(6 \times 4 \times 7 \times 5 \times 5)$

the temporal dimension for subsequent processing. For each of the 6 times indices, the output of convolution layer is then flattened in order to provide a 2 dimensional ten-

sor (red circular boxes on the sketch, of shape (6, 816) and (6, 208) for AROME and ARPEGE branches respectively), such that they have the same number of dimension as the

Station branch (whose input shape is  $(7,33)$ ). In each of the 3 branches, a set of temporal and static features are also provided at each time step  $t$  by tensor  $\mathbf{C}_{d,t}^s$ . These values are the time of the day  $t$ , the day of the year  $d$  and the location (latitude, longitude and altitude) of the station  $s$ .  $\mathbf{C}_{d,t}^s$  is then fed to a fully connected layer which encodes this information within a 16-dimensional tensor. For the station branch, a similar encoding of the position of each of the 10 neighboring sites,  $\mathbf{D}^s$  with respect to  $s$  is also provided. These tensors are then repeated at each of the input times (7 times for station data and 6 times for AROME and ARPEGE branches) and then concatenated to former input tensors or outputs of convolution layers.

As illustrated by green rectangles in Fig. 2, the so-obtained tensors are then processed through 2 or 3 stacked “Long Short-Term Memory” (LSTM) layers, a recurrent neural network architecture that is widely used to process sequential information (Goodfellow et al. 2016). The last outputs are finally entered into a fully connected layer. The outputs of each branch are finally concatenated into a single tensor to be processed by a final fully connected layer and then by the output layer, which is also a fully connected layer with a rectified linear unit (ReLU) activation that returns a vector of 6 positive values representing the predicted wind speeds at horizons  $h = 1, 2, \dots, 6$  hours. Hereafter we refer to such a model with 3 distinct branches separately devoted to leverage ground station, AROME and ARPEGE data, as the  $\mathcal{M}$  model. Within the notations of Eqs. (2) and (3), one has,

$$\widehat{\mathbf{V}}_{d,t+h}^s = \mathcal{M}(\mathbf{X}_{d,t}^s, \Theta) \quad (5)$$

with  $\mathbf{X}_{d,t}^s = [\mathbf{GS}_{d,t}^s, \mathbf{AR}_{d,t}^s, \mathbf{AP}_{d,t}^s, \mathbf{C}_{d,t}^s, \mathbf{D}^s]$ . We will also consider the restriction of the model to a single type of input, i.e., one that considers individually  $\mathbf{GS}_t^s$ ,  $\mathbf{AR}_t^s$  or  $\mathbf{AP}_t^s$  and their corresponding branch. When  $\mathcal{M}$  is reduced to its “ground station” “AROME” or its “ARPEGE” branch, the corresponding models will be denoted as respectively  $\mathcal{M}_{GS}$  model,  $\mathcal{M}_{AR}$  model and  $\mathcal{M}_{AP}$  model. Regarding the number of parameters to be learned in each model,  $\mathcal{M}$ , as previously described, consists of 262k parameters, while  $\mathcal{M}_{AR}$ ,  $\mathcal{M}_{AP}$ , and  $\mathcal{M}_{GS}$  contain 138k, 84k, and 39k parameters, respectively.

Let us finally notice that, as remarked previously, one can build  $\mathcal{M}'$ , a variant of  $\mathcal{M}$ , that outputs the wind speed probability distribution instead of its expected value:

$$\widehat{\rho}_{d,t+h}^s = \mathcal{M}'(\mathbf{X}_{d,t}^s, \Theta) \quad (6)$$

In this case, the last layer of  $\mathcal{M}'$  is a fully connected layer which outputs a  $(n,6)$  tensor, where  $n$  is the number of parameters necessary to define the chosen probability distribution  $\widehat{\rho}_{d,t+h}^s$ . In this work, we choose a law with  $n = 3$  parameters the so-called “Multifractal-Rice” (M-Rice) distribution, which has proven to be particularly suitable for

wind speed forecasting when compared to other distributions (Baggio and Muzy 2024). The M-Rice distribution has been introduced in Baïle et al. (2011) where the authors considered, inspired by the random cascade picture of fully developed turbulence, a Rice-distribution with a random scale parameter that follows, e.g., a log-normal distribution. Its density involves 3 parameters  $(\nu, \sigma^2, \lambda^2)$ . More details on this distribution and on the numerical method used to evaluate it are given in the Appendix.

### c. Deterministic and probabilistic approaches. Loss functions.

As explained in the previous section, we have the option to use the  $\mathcal{M}$  model to directly build the best prediction  $\widehat{\mathbf{V}}_{t+h}$  or, using the output of  $\mathcal{M}'$ , to compute it as the expectation under the best prediction of the probability law at each time according to Eq. (4). Let us describe these two options more precisely and the loss function one minimizes to estimate the parameters of  $\mathcal{M}$  or  $\mathcal{M}'$  respectively.

#### 1) DETERMINISTIC APPROACH

Since it is generally not possible to compute the conditional mean square involved in Eq. (1) at each prediction step, the most common approach is to compute the vector of model parameters  $\Theta$  that minimizes the time-averaged value of  $\mathcal{E}_{d,t}^{mse}$ , the conditional MSE defined in Eq. (1). Empirically, this involves finding the parameters  $\Theta$  that minimize a loss function that corresponds to the empirical MSE defined as:

$$\mathcal{E}^{mse} = N^{-1} \sum_{k=1}^N \left\| \mathbf{V}_{d,k}^s - \widehat{\mathbf{V}}_{d,k}^s \right\|^2 \quad (7)$$

$$= N^{-1} \sum_{k=1}^N \sum_{i=1}^H \left( \widehat{v}_{d_k, t_k+h_i}^{s_k} - v_{d_k, t_k+h_i}^{s_k} \right)^2 \quad (8)$$

where  $N$  is the number of available samples (in the training subset, see below) which corresponds to the number of different triplets “station”, “day” and “time of the day”  $(s,d,t)$  for which they are no missing data for building the observed velocity vector  $\mathbf{V}_{d,t+h}^s$  and the input tensors defined in the previous section. In that case, the last layer illustrated in Fig. 2, is, as previously anticipated, a fully connected layer with the ReLU activation function and that directly outputs a 6-dimensional positive vector representing the values of  $\widehat{\mathbf{V}}_{d,t+h}^s$  at 6 considered time horizon. The loss function we use is directly provided by Eq. (7).

#### 2) PROBABILISTIC APPROACH

As mentioned previously, in addition to the previous deterministic forecast approach (also called “single-point”), which consists in finding the best parametrization of the conditional mean wind speed value, one can try to estimate

directly the full conditional probability distribution from which the conditional mean is derived (see Eqs. (3), (4)).

Such an approach is usually referred to as probabilistic forecasting. It has become increasingly important in recent years as it captures not only the expected outcome but also uncertainties around this expectation and therefore provides notably insights into the likelihood of extreme events. A commonly used approach involves quantile-based methods which consists in directly estimating specific quantiles, such as the median or the 90th percentile, without assuming any particular probability distribution. On the other hand, parametric methods assume an underlying probability distribution and estimate its parameters to construct the forecast. These approaches are more parsimonious, offering a complete characterization of the forecast distribution, and they can integrate additional information, such as prior distributions, using frameworks like Bayesian inference. In this context, the challenge is to estimate, at each time step  $t$ , the vector of parameters  $\mathbf{\Pi}_t$  characterizing the conditional law  $f(y|\mathbf{\Pi}_t)$ . The most commonly used approach (see for example [Salinas et al. \(2020\)](#)) consists in considering the parameters that minimize the negative log-likelihood. Practically, this amounts to minimize the following loss function (also called *logarithmic score*):

$$\ell = -N^{-1} \sum_{k=1}^N \ln f(V_{d_k, t_k+h}^{s_k} | \mathbf{\Pi}_{t_k}) \quad (9)$$

where  $V_{d_k, t_k+h}^{s_k}$  is the observed surface wind speed at site  $s_k$ , day  $d_k$  and time  $t_k + h$ . For a multi-horizon prediction, i.e. when the goal is to predict wind speed at horizons  $h_1, h_2, \dots, h_H$ ,  $H \geq 1$  simultaneously, we can simply consider, as for the MSE loss in Eq. (7), the sum over all horizons of single horizon loss :

$$\ell_H = -N^{-1} \sum_{k=1}^N \sum_{i=1}^H \ln f(V_{d_k, t_k+h_i}^{s_k} | \mathbf{\Pi}_{t_k}) . \quad (10)$$

As discussed above, in this case the last layer of our neural network model  $\mathcal{M}'$  consists in a fully connected layer with output tensor of shape (3,6), corresponding to the 3 M-Rice parameters at the six time horizons. For each set of parameters, the conditional mean  $\widehat{V}_{d,t+h}^s$  is then obtained as the mean value of the corresponding M-Rice law which is provided by Eq. (A2) in Appendix.

#### d. Training, validation and test sets, model's hyperparameters

As detailed in Sec. 2, the MeteoNet dataset covers a period of 3 years from 01-01-2016 to 31-12-2018. The input data in the  $\mathcal{M}$ ,  $\mathcal{M}'$  models, is built from (normalized) data for each station  $s$ , day  $d$  and time  $t$  of the day ( $t$  are expressed in multiple of hours and are such that  $t \leq 18$  UTC).

Let us refer to such a triplet  $(s, d, t)$  as a *key*. The stations we have considered in this work are the stations such that the number of available keys is greater than 2000, meaning that over all possible 17,520 keys for the whole period, at least 2000 are such that there is no missing data among all data presented in Table 1. Only 278 stations among the 478 available Meteonet stations satisfy this criterion and are the ones used in this study. This corresponds to a total number of keys,  $N \simeq 3.5 \times 10^6$ . For learning purposes, this global sample is divided in 3 subsets: a training subset devoted to training with 70 % of data, a validation subset to monitor training and control the choice of parameters and hyper parameters of size 20 % of the total size and finally a test subset used to provide an unbiased assessment of the model's performance with the remaining 10 % of the dataset. We remark that when on a given day  $d$  and time  $t$ , data from a station  $s$  are included in the training set, and data from the same station (or from a nearby station  $s'$ ) at a nearby time are included in the validation set, this can lead to overfitting. This occurs because similar situations appear in both the training and validation (or test) sets. To prevent this, the dataset is split by day: all data from a specific day are assigned exclusively to either the training, validation, or test set, ensuring no overlap across subsets.

In this work, we will also experiment fine-tuning a model in order to optimize it for a specific station. Fine-tuning a neural network involves taking a pre-trained model and further training it on a specific subset of data, allowing it to adapt to localized conditions and improve predictive accuracy for a particular domain or task ([Quinn et al. 2019](#)). Fine-tuning is often used when the general structure of the model is suitable but improvements are needed for specific data characteristics. It is different from the so-called "transfer learning" that refers to leveraging a model pre-trained on a large dataset and reusing its learned features for a new task. Transfer learning typically involves replacing or adding new layers to adapt the model to the new problem, while fine-tuning focuses on further optimizing the pre-trained model for better performance on the target dataset. To fine-tune the model for a specific station  $s$ , we initialize it with the parameters obtained from the global training phase. The fine-tuning process then involves further training the model using the same loss function, as defined in Eq. (10), but restricting the training data to that of station  $s$  exclusively. To mitigate the risk of overfitting, the training data used for fine-tuning consist solely of the subset of the global training set corresponding to station  $s$ . Similarly, the validation and test sets are derived as subsets of the global validation and test datasets, containing only data associated with the station  $s$ .

Hyperparameters are parameters that govern the learning process and the configuration of the model. Unlike model parameters, they are not learned during the training phase, but are chosen before the learning process begins. While many hyperparameter optimization techniques that



TABLE 2. Learning Hyperparameters used in our study

Parareter	Value
Optimizer	Adam
Learning rate	0.001
Batch size	512
LSTM Dropout level	0.02

systematically explore configurations to improve model performance exist, such as grid search or random search, we did not apply such optimization methods in our work. Instead, we experimented with a few values for layer configurations and learning parameters.

The model configuration is shown in Fig. 2, and learning parameters are in Table 2. Since hyperparameters were not optimized on the validation set, we expect similar performance between validation and test sets. Our observations confirm this, with results within a few percentage points.

#### e. Metrics

In order to assess the forecasting performance of a model, the most commonly used metrics is the so-called Root-Mean-Squared-Error (RMSE), that is defined as:

$$\text{RMSE} = \sqrt{\frac{1}{NH} \sum_{k=1}^N \sum_{i=1}^H (\widehat{V}_{d_k, t_k+h_i}^{s_k} - V_{d_k, t_k+h_i}^{s_k})^2} \quad (11)$$

where  $k$  belongs to either the validation or test subset. In any case,  $N$  represents the number of samples of the considered subset and  $H$  stands for the number of prediction horizons ( $H = 6$  in our study). RMSE corresponds to the empirical deviation (in  $m s^{-1}$ ) of observed velocity as respect to the prediction averaged over all stations, all days, all times and all horizons. Let us emphasize that, since our goal is to compare models providing single-point predictions, we treat model  $\mathcal{M}'$  that provides a probabilistic forecasting as an intermediate step for generating deterministic predictions. Such a model is also evaluated using the RMSE metrics. Probabilistic metrics (e.g., log-score, CRPS; see [Baggio and Muzy \(2024\)](#)) will be explored in a future study.

In section 4-2 we study the performance of the model in forecasting extremes. The occurrence or non-occurrence of an extreme wind value is given by a binary variable  $I_{d,t}^s$ , such that  $I_{d,t}^s = 1$  if the event occurs, while  $I_{d,t}^s = 0$  otherwise. Then the quality of binary forecasts  $\widehat{I}_{d,t}^s$  needs to be evaluated by a relevant metric. This is usually referred to as a “classification problem” (as opposed to a “regression problem” as formerly considered). In that case, one can use a variety of metrics (or skill scores), depending

upon which aspect of the prediction one wants to optimize. We can refer the reader to [Jolliffe \(2004\)](#) (see also [Wilks \(2019\)](#)) for a comprehensive review on the topic. Among all possible scores, the Peirce Skill Score (PSS) is a widely used metric for evaluating the performance of a binary classification model, particularly in the context of severe weather prediction. It is defined as:

$$\text{PSS} = \text{HR} - \text{FA} \quad (12)$$

where HR stands for “Hit Rate” and FA for “False Alarm Rate”. These rates are derived from the contingency table of predictions, where the  $N$  forecast/observation pairs  $(\widehat{I}_{d,t}^s, I_{d,t}^s)$  are divided in true positives TP, false positives FP, false negatives FN and true negatives TN (we thus have  $\text{TP} + \text{FP} + \text{FN} + \text{TN} = N$ ). More specifically,  $\text{HR} = \frac{\text{TP}}{\text{TP} + \text{FN}}$  corresponds to the fraction of correctly predicted positive events, while  $\text{FA} = \frac{\text{FP}}{\text{TN} + \text{FP}}$  is the fraction of wrongly predicted, i.e. predicted as positive, negative events. Unlike accuracy-based scores, PSS accounts for both missed events (false negatives) and false alarms (false positives), providing a balanced assessment of quantifying model performance. Moreover, this score is particularly suitable for forecasting extremes as it weights more strongly correct yes forecasts of rare events, thus discouraging artificial distortions towards the more common class. The PSS ranges from  $-1$  to  $1$ , with  $\text{PSS} = 1$  corresponding to a perfect forecast and  $\text{PSS} = 0$  corresponding to unskilled, i.e., purely random, forecast. This means that a negative PSS value reflects prediction performance that is worse-than-random. Another score commonly used when forecasting rare events ([Jolliffe 2004](#)) is the Critical Success Index (CSI), also known as Threat Score. It is defined as:

$$\text{CSI} = \frac{\text{TP}}{\text{TP} + \text{FP} + \text{FN}}, \quad (13)$$

corresponding to the ratio between the times  $I_{d,t}^s = 1$  has been forecasted correctly and the total number of times the event either happened, has been forecasted or both. The maximum value for CSI is  $1$ , while the lowest possible value is  $0$ . As TN are not considered in 13, this metric is not artificially inflated by correct forecasts of the more common “no” event. However, contrary to PSS, it is not an equitable metric, which makes comparisons between binary events with different frequency of occurrence not straightforward. In the following, we refer mostly to the PSS when assessing performance, however, we will show some results in terms of CSI as well.

#### f. Baseline models

In order to compare the performance of previous neural network models with alternative approaches, we consider various simple or natural baselines. The first model we consider corresponds to the raw output directly provided

by the NWP regional model, namely the AROME model. For a given site  $s$ , some given day  $d$  and time  $t$ , at the lead time  $h$ , we use the wind speed values from the closest grid point in AROME at time  $t+h$ . This will be referred to as the “Raw AROME” prediction. Although, as discussed in the introduction, such raw predictions can often exhibit some bias and can be improved through different post-processing approaches, it is the simplest baseline model one can use for reference. Along the same line we also consider “Raw ARPEGE” as the prediction provided by the global ARPEGE model at the grid point closest to the considered site. Given that AROME predictions are downscaled from ARPEGE, it is expected that AROME will deliver superior performance over ARPEGE. Another model that is usually considered as a reference model for surface wind speed is the so-called “Persistence”, which consists in considering the last measured value as the best forecast. Mathematically, this amounts to assuming that the wind speed is a Martingale random process. Finally, for the sake of completeness, we consider the class of linear models as last comparative models. Such models can notably be considered as the most basic neural network with a single fully connected layer with a linear output and which takes the past observed wind speed values as input. This model will be referred to as  $\mathcal{L}$  (for linear) model.

#### 4. Results

##### a. Hybrid model vs various baselines over all station sites

##### 1) COMPARISON WITH BASIC MODELS: RAW AROME PREDICTION AND PERSISTENCE MODELS

TABLE 3. RMSE relative improvement of  $\mathcal{M}$  as respect to baseline models at horizons 1 and 6 hours

Baseline / horizon	1h	6h
Persistence	6.2 %	45 %
Linear	2 %	37 %
Raw AROME	37 %	28 %
Raw ARPEGE	49 %	41 %

The comparative performances in terms of RMSE of the  $\mathcal{M}$  model and the various baseline models are reported in Fig. 3. These results correspond to the RMSE evaluated over the test set for all 278 stations in the MeteoNet dataset for prediction horizons  $h = [1, 2, 3, 4, 5, 6]$  hours. One can see that the  $\mathcal{M}$  model significantly outperforms all baselines for all horizons, as highlighted in Table 3 for horizons 1 and 6 hours. We see that Linear ( $\mathcal{L}$ ) and Persistence models based on station data provide good performances at very short time horizons but quickly become less reliable as the forecasting horizon increases. On the other hand, as anticipated in the discussion of Sec. 3-a, we observe that raw

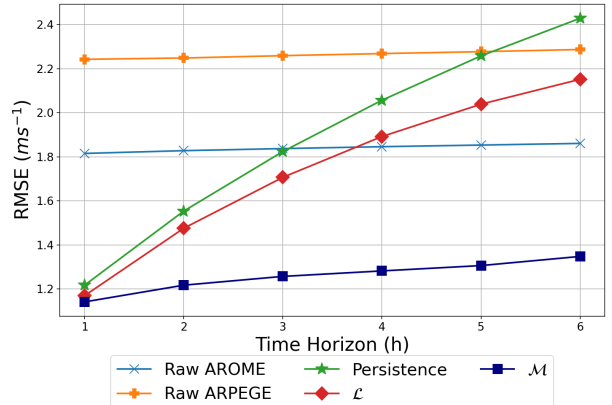


FIG. 3. Comparison of  $\mathcal{M}$  model performance as respect to various baseline models described in the text. The RMSE over the test sample is reported for each prediction horizon.

NWP predictions (AROME and ARPEGE) errors hardly vary with horizon. We also observe that, as expected, the regional, high-resolution AROME model performs better than the global ARPEGE model. AROME becomes better than a regression of station data at horizons greater than 3 h. However, both models are surpassed by  $\mathcal{M}$ , even at largest time horizons. This clearly demonstrates how  $\mathcal{M}$ , which can be considered as a kind of post-processing method, can greatly improve the prediction accuracy of raw NWP forecasts by leveraging multiple sources of input data and correcting bias inherent to these models.

Fig. 4 illustrates model predictions for the specific case of two ground station sites in Corsica: Ajaccio and Bonifacio. In Ajaccio, we observe a pronounced annual oscillation related to the coastal breeze regime, whereas in Bonifacio, wind speeds are more intermittent and wind gusts more intense. In both subplots, we present the values of 6-hour ahead forecasts from the AROME and  $\mathcal{M}$  models at a fixed time of day  $t_d = 1100$  UTC (the corresponding initial time is therefore  $t = t_d - h = 0500$  UTC) for all days over the 2016–2018 period. For the sake of clarity, the plots include all three sub-periods (training, validation, and test subsets), which may result in slightly overestimated model performance compared to its actual values. We see that both model predictions closely align with ground truth values at both locations for all time periods. It can be however remarked that AROME model slightly underestimates wind speeds, particularly during winter, at both sites (in Fig. 4, orange squares are more likely to be observed under black solid lines than blue circles). These observations highlight the need for some bias correction in raw numerical weather prediction (NWP) outputs, reinforcing the importance of post-processing techniques in improving forecast accuracy.

It is important to note that, beyond the average results presented in Fig. 3, the RMSE-based forecasting perfor-

mance of the  $\mathcal{M}$  model varies significantly across stations. This variability stems from the strong spatial variability in site-specific weather conditions, particularly mean wind speed. As shown in Fig. 5, there is a clear linear dependence between RMSE and mean wind speed estimated at each site over the full 3 years period, with higher mean value leading to larger prediction error.

## 2) COMPARISON WITH SINGLE BRANCH MODELS

In Fig. 6 are displayed, as a function of the horizon, the RMSE performances of the  $\mathcal{M}$  model comparatively to  $\mathcal{M}_{AR}$ ,  $\mathcal{M}_{AP}$  and  $\mathcal{M}_{GS}$  models that respectively process AROME, ARPEGE and Ground Station input data without other branches. We first see that  $\mathcal{M}$  predictions are the best among all alternatives for all times horizons. Let us also observe, by comparing the results of Figs 3 and 6, that post-processing NWP inputs, whether AROME or ARPEGE, with a neural network model significantly reduces their error. Specifically, the RMSE for  $\mathcal{M}_{AR}$  predictions is reduced by approximately 27 % compared to raw AROME predictions, while the RMSE for  $\mathcal{M}_{AP}$  predictions is reduced by about 36 % compared to raw ARPEGE predictions.  $\mathcal{M}_{AR}$  model associated with AROME remains better than  $\mathcal{M}_{AP}$ , the one associated with ARPEGE, even if the difference between the two models is reduced as compared to the raw predictions. In both models, as before and as expected from discussion in Sec. 3-a, the error only slightly depends on the time horizon. On the other hand, as remarked previously, the performance of  $\mathcal{M}_{GS}$ , the model relying exclusively on past observations at ground station and its surrounding sites, strongly depends on the horizon and clearly decreases as the horizon increases.

## 3) FEATURE IMPORTANCE ANALYSIS

In the previous paragraph, we have seen that the model  $\mathcal{M}$ , which integrates all three data sources, consistently outperforms the best individual model at every forecast horizon. The model leverages the strengths of each model at each time horizon, optimizing performance across all forecasts. In order to assess the contribution of each feature to the reduction in final RMSE, we adopt the approach outlined in Rasp and Lerch (2018), which is based on a method originally proposed by Breiman (2001) for random forest models. This method simply consists for a given input feature or group of features, in randomly shuffling the corresponding data among a given mini-batch sample. The main advantage of this method is its relative simplicity and the fact that it does not require retraining the model. This is not the case of the approach used by Marcille et al. (2024), which involves analyzing the impact of a specific subset of features by removing it from the original input and run a new training phase within this configuration.

If  $\mathcal{E}_{ref}[h]$  is the mean-squared error associated with the reference model at a given horizon  $h$  and  $\mathcal{E}_F[h]$  is the

mean-squared error at horizon  $h$  obtained when randomly shuffling the input feature (or group of input features)  $F$ , then  $S_F[h]$ , an ‘‘importance score’’ of  $F$  at horizon  $h$  can be defined as:

$$S_F[h] = \frac{\sqrt{\mathcal{E}_{ref}[h]} - \sqrt{\mathcal{E}_F[h]}}{\sqrt{\mathcal{E}_{ref}[h]}}.$$

In Fig. 7 are reported the importance score at horizons  $h = 1$ ,  $h = 3$  and  $h = 6$  hours for each feature in the  $\mathcal{M}$  model computed on the test sample for the whole dataset. One can see that NWP and station wind components inputs are, by far, the most important features. Among other features, the relative humidity predicted by AROME model and the temporal features (date, hour of the day) have the most significant impact of the prediction performances. As far as horizons are concerned, there is no clear trend in AROME feature importance whereas ARPEGE wind feature become more important as the horizon increases. This is not surprising since ARPEGE is a global model that is designed to capture large scale features several days ahead. On the other hand, past station features become less important for longer horizons as compared to shorter ones. Models based on observed past weather conditions at the target site and its surrounding ground stations are more likely to be useful at small horizons than for longer ones. It is noteworthy that for both AROME and ARPEGE temperature data have more impact on the prediction quality than pressure data. This may be reminiscent of the correlation of the wind components with thermal breezes as observed by Marcille et al. (2024) for the meridional wind at the coastal station they analyzed.

## 4) THE BENEFITS OF A PROBABILISTIC APPROACH

In Fig. 8, we compare the RMSE observed on the test set for the  $\mathcal{M}$  model (blue (■) symbols) and the  $\mathcal{M}'$  model (red (●) symbols). Recall that the latter is designed to predict the parameters of the M-Rice probability distribution for the wind speed over the next six hours. At each time step, one can then compute, for any given forecasting horizon, the conditional mean using Eq. (A2) and then the resulting MSE over the validation or the test samples. As it can be observed in Fig. 8, whatever the considered horizon the probabilistic model ( $\mathcal{M}'$ ) provides slightly better forecasts than the deterministic version ( $\mathcal{M}$ ). A priori, the model designed to optimize directly the empirical MSE ( $\mathcal{M}$ ) is expected to provide better results in terms of MSE as compared to any other one.

It appears, from Fig. 8, that parametrizing directly the conditional mean is less efficient than trying to estimate it through the probability law it is associated with. Let us observe that this is even more true as the forecast horizon increases. Moreover, as advocated previously, probabilistic forecasts offer valuable insights beyond a single-point

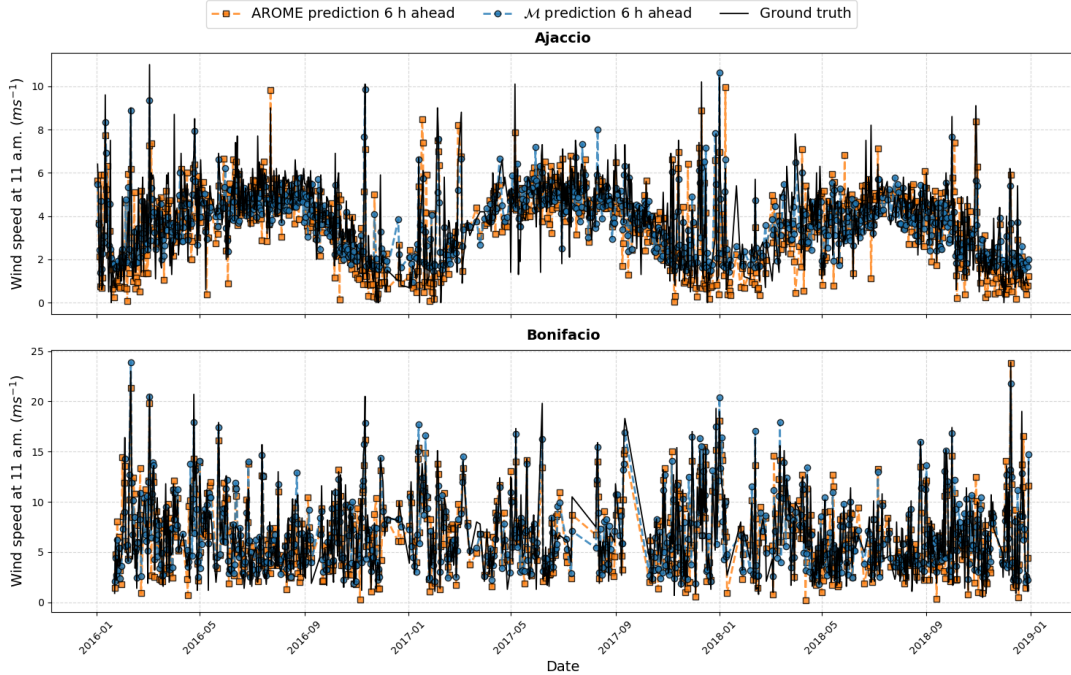


FIG. 4. Illustration of the  $\mathcal{M}$  model and the raw AROME forecasting performances in Ajaccio and Bonifacio for  $h = 6$  h ahead prediction of wind speed value at time of the day  $t_d = t + h = 1100UTC$ . At first sight performances are comparable but one can see that the regional NWP model is slightly biased towards small wind speed values. One can also observe strong seasonal effects in Ajaccio where breeze regimes are much more important than in Bonifacio site.

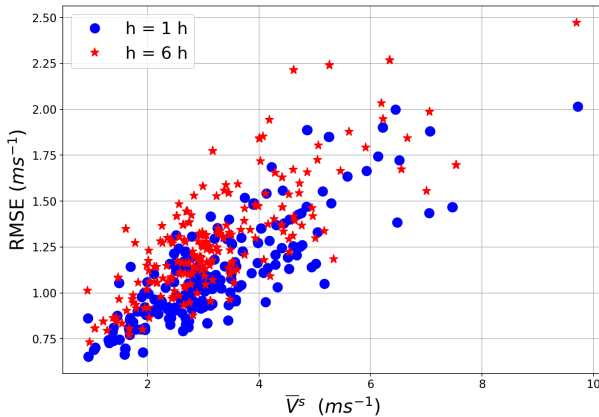


FIG. 5. RMSE associated with the  $\mathcal{M}$  prediction as a function of the station mean wind speed value (estimated over 3 years)  $\bar{V}^s$  for all sites for horizons  $h = 1$  hour and  $h = 6$  hours.

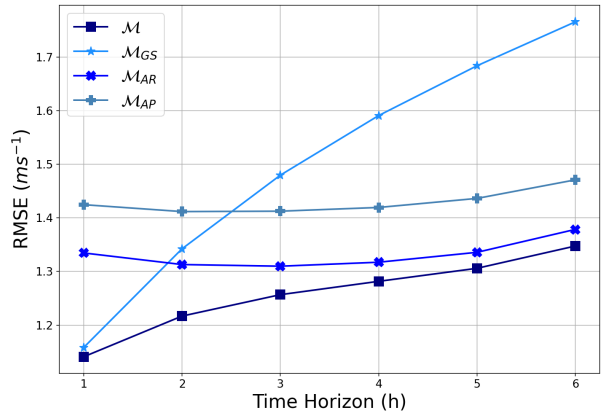


FIG. 6. Comparison of  $\mathcal{M}$  model performance as respect to  $\mathcal{M}_{AR}$ ,  $\mathcal{M}_{AP}$  and  $\mathcal{M}_{GS}$  models. The RMSE over the test sample is reported for each prediction horizon.

prediction. They provide the entire probability distribution, offering the possibility to compute various risk measures and facilitating decision-making tailored to specific objectives. Even for single-point prediction, as considered in this paper, if one uses different metrics, the probability law can provide more efficient prediction than the MSE. For example, if one aims at minimizing another metrics

instead of the MSE (e.g. the mean absolute error), there is no need to perform another training of the model since it suffices to compute, for each station and for each time  $t$ , the value that optimizes this metrics as the best forecast instead of the conditional mean value (e.g., the conditional median). In Sec. 4-b-2, we will see that in the case of extreme wind occurrence prediction, high quantile values

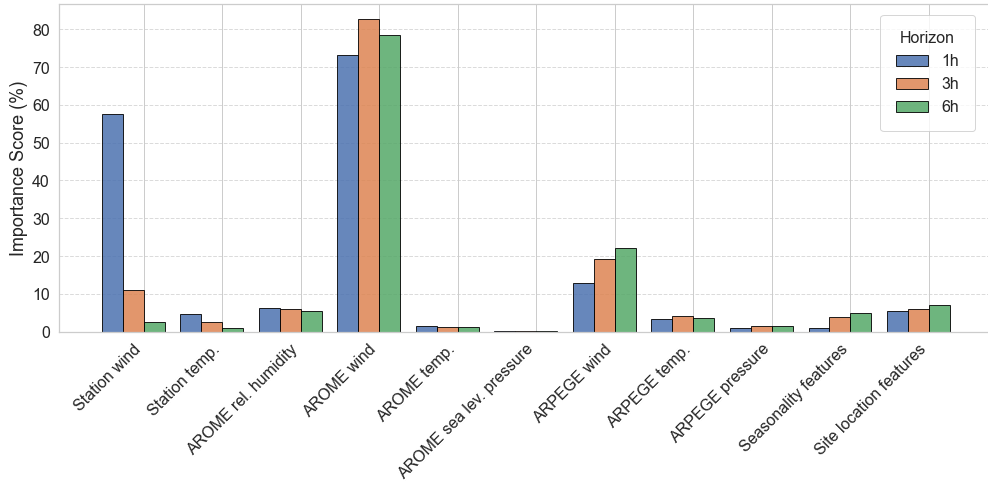


FIG. 7. Importance score  $S_F$  for each (class of) input feature  $F$  at horizons 1 hour, 3 hours and 6 hours

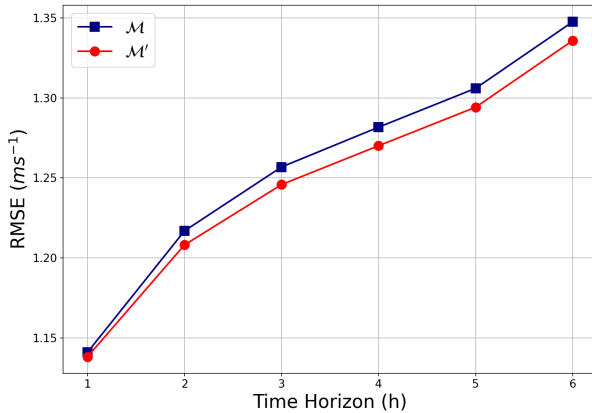


FIG. 8. Comparison of  $\mathcal{M}$  (■) and  $\mathcal{M}'$  model (●) RMSE for all stations as a function of the forecasting horizon.

threshold exceedances provide a very good predictor which outperforms significantly the deterministic predictions.

### b. Focus on sites in Corsica

In this section, our aim is to focus more specifically on a particular subset of locations, that is the 21 ground stations in Corsica that have sufficient available data for analysis. The precise locations and names of these stations are shown in Fig. 1(b).

#### 1) FINE TUNING THE GLOBAL MODEL FOR EACH STATION

As noted in the Introduction, Corsica is a Mediterranean island characterized by a highly heterogeneous, complex, and mountainous terrain, subject to diverse weather conditions. These factors contribute to significant spatial variability in wind regimes. Consequently, the performance of

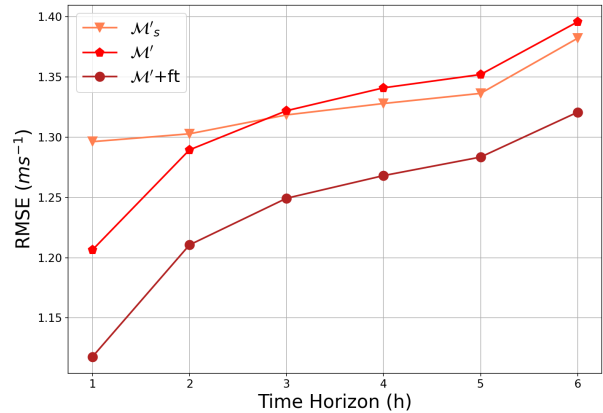


FIG. 9. Comparison of the average RMSE over the 21 Corsican stations with and without fine-tuning. Symbols (●) represent the  $\mathcal{M}'$  model as optimized globally (without any fine-tuning), (▼) the average RMSE of the  $\mathcal{M}'_s$  model which is the  $\mathcal{M}'$  model fully optimized for each station without any peculiar initialization and the symbols (●) represent the average RMSE of the fine-tuned  $\mathcal{M}'$  model.

the model (e.g.,  $\mathcal{M}'$ ), which has been globally trained using all stations, is expected to vary significantly across sites. To address this challenge and enhance model performance, we explore the possibility of fine-tuning its parameters for each station according to the methodology described in Sec. 3-d.

Figure 9 presents, using symbols (●), the RMSE for each forecast horizon, obtained as the square root of the averaged MSE of the fine-tuned model across the 21 stations reported in Fig. 1(b). For comparison, the figure also includes the analogous RMSE obtained without model retraining, i.e., corresponding to the globally optimized model  $\mathcal{M}'$  (symbols (●)). We have also computed the

TABLE 4. Comparative RMSE for models  $\mathcal{M}'$  and  $\mathcal{N}$  for horizons 1,3,6 hours.

Site	Horizon (h)	Model $\mathcal{N}$ ( $ms^{-1}$ )	Model $\mathcal{M}'$ ( $ms^{-1}$ )	Improvement (%)
Ajaccio	1	1.01	0.95	5.9
	3	1.15	1.00	13.0
	6	1.26	1.07	15.1
Lucciana	1	1.08	1.03	4.6
	3	1.24	1.16	6.5
	6	1.35	1.22	9.6
Figari	1	1.21	1.15	5.0
	3	1.41	1.27	9.9
	6	1.56	1.32	15.4
Renno	1	0.97	0.92	5.2
	3	1.10	1.00	9.1
	6	1.14	1.05	7.5

average RMSE of  $\mathcal{M}'_s$ , the “locally trained” models that corresponds to the model  $\mathcal{M}'$  which is fully trained specifically for each station without providing any peculiar initial weights (symbols  $\blacktriangledown$ )).

The results clearly show that fine-tuning improves performance as respect to both the globally trained model and locally trained models. It is worth mentioning that the improvement of fine tuned model as respect to the global one is consistently observed for all stations and all horizons. The performance gain compared to the model  $\mathcal{M}'_s$ , fully trained on data from a single station (symbols  $\blacktriangledown$ ) is even more pronounced at shorter time horizons. Training  $\mathcal{M}'$  for a given station  $s$  in isolation, without leveraging the optimal weights obtained from the full set of stations, leads to poorer performance on the validation and test subsets. This degradation can be primarily explained by overfitting, as the amount of training data available for a single station is significantly smaller than that of the entire Southeast station network.

Let us end this section with the results of Table 4 which compares the performance of the fine-tuned  $\mathcal{M}'$  model against a neural network model introduced in Baile and Muzy (2023) and trained using the dataset described in Section 2-b, which spans a longer period than MeteoNet (2011-2020). This model has an architecture which is similar to the  $\mathcal{M}_{GS}$  model described in Sec. 3-b and takes, as input data, the last few hours observations from the target station and its 15 neighboring stations. This baseline model will be referred to as  $\mathcal{N}$ . Due to its relatively simple structure,  $\mathcal{N}$  is trained and optimized separately for each station. The reported RMSE values for both models are computed over the same evaluation set to ensure a fair comparison. The results show that, across all sites and forecast horizons,  $\mathcal{M}'$  consistently outperforms  $\mathcal{N}$ , despite being trained on a significantly shorter time period. Fur-

thermore, as expected, the performance gap widens with increasing forecast horizons. This highlights the advantage of  $\mathcal{M}'$ , which integrates numerical weather prediction (NWP) data, over  $\mathcal{N}$ , which relies solely on past observed data. It also shows the interest of fine tuning using a shorter period when one cannot train a local model using a long enough period.

## 2) PREDICTING STRONG WIND OCCURRENCES

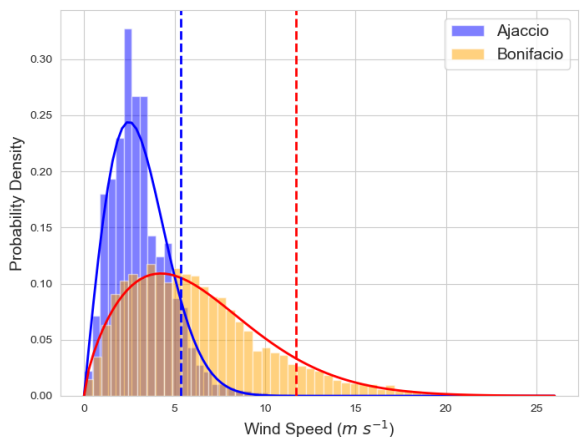


FIG. 10. Wind speed distributions observed at the Ajaccio (blue) and Bonifacio (orange) ground stations. Solid lines represent the corresponding Weibull distribution fits. Dashed lines indicate the 90 % quantiles for both locations.

One possible appealing application of our approach, which is both local and probabilistic, is to predict the occurrence of local strong wind regimes. Indeed, the notion of

strong wind velocity is very dependent on the site. In Fig. 10, the observed wind velocity distributions in Ajaccio and Bonifacio sites are illustrated. We see that the wind distribution in Ajaccio is concentrated around low wind speeds, whereas in Bonifacio, the distribution is broader, indicating a higher likelihood of strong wind events. This reflects the distinct wind climates of the two locations: Bonifacio experiences significantly stronger and more turbulent winds. This is primary due to its exposure in the Strait of Bonifacio that channels and accelerates winds, particularly when they are northwesterly like Mistral. The high limestone cliffs and surrounding hills also induce sudden wind gusts, direction shifts, making the wind highly variable near the coast. In contrast, Ajaccio is more sheltered within its gulf, resulting in generally milder winds, with only occasional strong gusts from dominant regional wind patterns (notably during Mistral and Libeccio episodes in autumn and winter). The concept of “strong winds” can therefore vary significantly depending on the location. A practical approach to defining strong winds is to use a threshold based on a quantile of the specific wind speed distribution of each site  $s$ . This approach relates to an estimate of the potential wind impacts accounting for the adaptation of local infrastructure (Klawa and Ulbrich 2003). The dashed lines in Fig. 10 represent the 90 % quantile values for both locations, meaning that only 10 % of wind occurrences exceed these thresholds at their respective sites.

Within this context, predicting strong wind events at a given location amounts to forecasting the occurrence of threshold exceedances, where the threshold corresponds to a high quantile relative to the site’s wind climatology. Let us denote  $Q^s(\rho_C, q)$  the quantile of probability level  $q$  associated with the climatological distribution  $\rho_C(V)$  relative to station  $s$ , i.e., the value such that:

$$\int_0^{Q^s(\rho_C, q)} \rho_C(V) dV = q. \quad (14)$$

Let  $\mathcal{H}$  be the Heaviside function and define the function:

$$\mathcal{H}_{s,q}(z) = \mathcal{H}\left(z - Q^s(\rho_C, q)\right) = \begin{cases} 1 & \text{if } z \geq Q^s(\rho_C, q), \\ 0 & \text{otherwise.} \end{cases} \quad (15)$$

For any site  $s$ , at time  $t$  on day  $d$ , we consider the binary variable  $I_{d,t}^s$  defined as

$$I_{d,t}^s = \mathcal{H}_{s,q}(V_{d,t}^s). \quad (16)$$

This variable indicates the occurrence of strong wind speeds, characterized by exceeding a given threshold in the tail of the site’s climatological distribution. Predicting strong events occurrence thus amounts to predict the value of  $I_{d,t+h}^s$  at each time  $t$ , day  $d$ , for each station  $s$  and horizon  $h$ .

In order to assess the quality of the prediction of  $I_{d,t}^s$ , we use PSS defined in Eq. (12). One of its main advantages is that it is unaffected by class imbalance, making it particularly useful in forecasting of strong wind episodes.

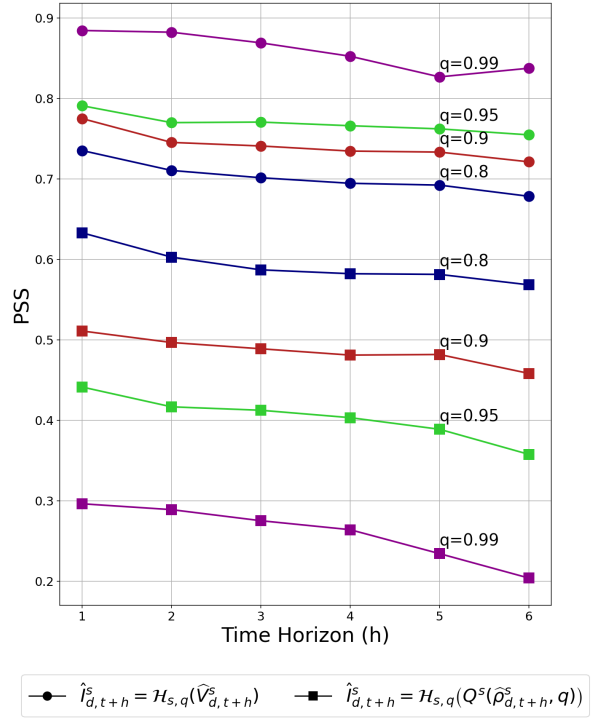


FIG. 11. Predicting strong event occurrences: Symbols (■) represent deterministic predictions (based on mean value) while symbols (●) represent probabilistic based prediction (based on quantile value). For each type of prediction, 4 curves are represented corresponding to a probability level  $q = 0.8, 0.9, 0.95, 0.99$  that is used to define  $I_{d,t}^s$  according to Eq. (16).

In the case of a single point prediction at site  $s$ , day  $d$  and time  $t$ ,  $\widehat{V}_{d,t}^s$  as provided, for instance, by the  $\mathcal{M}$  model in order to minimize the empirical MSE error or by the  $\mathcal{M}'$  model in order to minimize the estimated conditional MSE, a natural predictor of  $I_{d,t+h}^s$  is

$$\widehat{I}_{d,t+h}^s = \mathcal{H}_{s,q}(\widehat{V}_{d,t+h}^s). \quad (17)$$

On the other hand, for any station  $s$ , the model  $\mathcal{M}'$  provides, at each  $t$  and for each horizon  $h$ , an estimate of  $\widehat{\rho}_{d,t+h}^s$ , the condition probability distribution of  $V_{d,t+h}^s$  from which one can infer the conditional level- $q$  quantile,  $Q^s(\widehat{\rho}_{d,t+h}^s, q)$  as in Eq. (14). In this case, as shown in Mason (1979) (see also Jolliffe (2004)), one can explicitly build the “best” predictor of  $I_{d,t+h}^s$ , in the sense it is the one that maximizes the PSS, as:

$$\widehat{I}_{d,t+h}^s = \mathcal{H}_{s,q}\left(Q^s(\widehat{\rho}_{d,t+h}^s, q)\right). \quad (18)$$

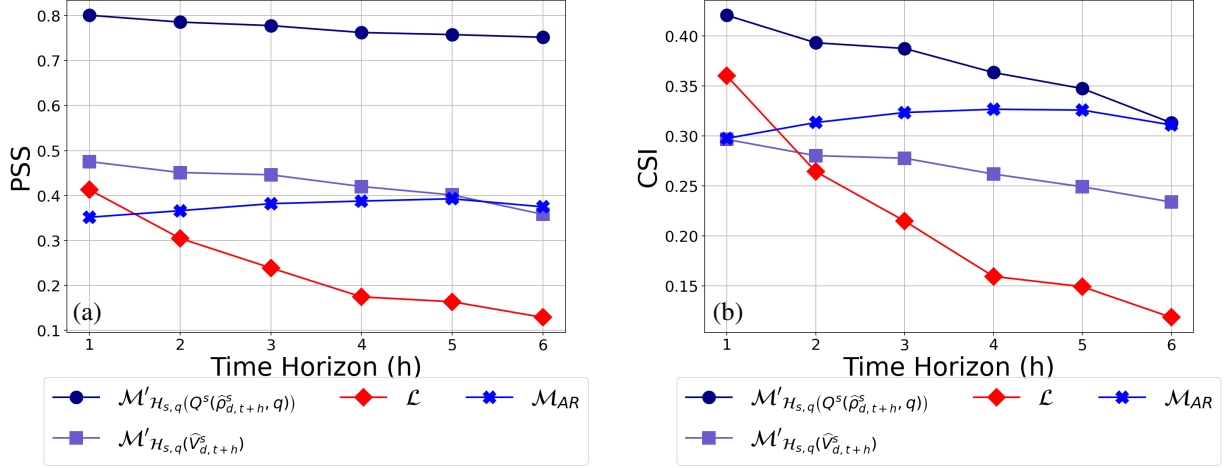


Fig. 12. (a) Predicting strong event occurrences: comparisons of three models for predicting the exceedance of 95 % quantile of each site. (●) symbols represent the fine-tuned  $\mathcal{M}'$  model with predictor (18), (■) symbols represent the fine-tuned  $\mathcal{M}'$  model with predictor (17), (✱) symbols represent the prediction from  $\mathcal{M}_{AR}$  model and the (◆) represent the performance of the linear prediction, where a linear regression over past observed wind speeds at the station and its surrounding stations is optimized, individually for each station, in order to minimize MSE. (b) The same model are compared in terms of CSI where the level  $q = 0.33$  is used in (18)).

Such a prediction is different from the previous one in Eq. (17) since the expected conditional mean value  $\hat{V}_{t+h}^s$  has been replaced by the level- $q$  conditional quantile. In Fig. 11 we compare the PSS value, averaged for all 21 Corsican stations, as obtained on the test and validation periods, for the fine-tuned  $\mathcal{M}'$  model when one use estimators (17) and (18) for the extreme events occurrence. Comparison is performed for all horizons  $h = 1, 2, 3, 4, 5, 6$  hours and threshold values corresponding to  $q = 0.8, 0.9, 0.95, 0.99$  station climatology quantiles. The PSS performance is averaged across both the validation and test periods to provide more representative samples of extreme events, which becomes increasingly important as the quantile considered increases. We clearly observe that the method leveraging probabilistic prediction to estimate conditional quantiles, as in (18), achieves significantly better performance, particularly for extreme quantiles. As the threshold value  $Q^s(\rho_C, q)$  increases (i.e., as  $q$  rises from 0.8 to 0.99), the predictive performance of the conditional mean  $\hat{V}_{t+h}^s$  deteriorates sharply, whereas the performance of the conditional quantile prediction  $Q^s(\hat{\rho}_{t+h}^s, q)$  improves. In other words, probabilistic forecasting effectively captures extreme wind speed occurrences, outperforming the standard mean squared error (MSE)-based predictor.

Let us finally assess the performances of the finely tuned probabilistic model  $\mathcal{M}'$  to predict strong wind speeds by comparing it (i) to its "deterministic" counterpart, that is the fine tuned model  $\mathcal{M}'$  using the mean value as predictor, (ii) to a linear model  $\mathcal{L}$  (see Sec. 3-f) optimized for each station and (iii) to the model  $\mathcal{M}_{AR}$  defined in Sec. 3. The results for all sites in Corsica over both validation and test intervals are presented in Fig. 12 in the case

$q = 0.95$ . Performance measures are assessed using both PSS (Fig. 12(a)) and CSI metrics defined in 3-e (Fig. 12(b)). In the latter case, as advocated in Jolliffe (2004), the optimal probability threshold in Eq. (18) is no longer  $q = 0.95$  as for PSS but has to satisfy  $q = \frac{CSI}{1+CSI}$ , which corresponds to  $q \approx 0.33$  for an expected CSI around 0.5. Regarding the PSS, one observes in Fig. 12(a) that the ability of all the deterministic baseline models to predict strong wind events is significantly lower than that of the  $\mathcal{M}'$  model with an optimal threshold value. Incidentally, we can see that the model  $\mathcal{L}$  outperforms  $\mathcal{M}_{AR}$  at short time horizons. However, its performance declines rapidly as the forecast horizon increases which contrasts with  $\mathcal{M}'$  and  $\mathcal{M}_{AR}$  models that both maintain stable predictive skill over time. Similar results can be observed in Fig. 12(b) for the CSI, although the benefits of  $\mathcal{M}'$  are less significant, particularly at largest horizons. This maybe due to the fact that the chosen threshold  $q = 0.33$ , the same for all stations, is suboptimal in that case.

## 5. Summary and prospects

This study introduces a hybrid neural network model for short-term (1-6 hours ahead) surface wind speed forecasting, combining Numerical Weather Prediction (NWP) data with observational data. The model leverages the MeteoNet dataset, which includes global ARPEGE and high-resolution AROME NWP data and observations from ground weather stations in Southeast France, with a focus on the Mediterranean island of Corsica. The proposed model, denoted as  $\mathcal{M}$  (or  $\mathcal{M}'$  for its probabilistic version), integrates these three sources of input data within a neural



network architecture that combines LSTM units to process temporal information and convolutional layers to capture spatial patterns.  $\mathcal{M}$  is trained to minimize the mean squared error (MSE) for deterministic forecasts while, for probabilistic forecasts,  $\mathcal{M}'$  predicts the parameters of a Multifractal-Rice (M-Rice) distribution, achieved by minimizing the associated negative log-likelihood.

We find that our hybrid model significantly outperforms baseline models, including raw NWP predictions (AROME and ARPEGE), persistence models, and linear regression models, across all forecast horizons (1-6 hours). When analyzing feature importance, we observe that wind components from NWP models are the most important features for prediction accuracy. AROME features remain consistently important across all horizons, while ARPEGE features gain importance at longer horizons. Direct observations from ground stations are more useful for forecasts at shortest horizons. We also show the probabilistic version of the model slightly outperforms the deterministic version in terms of RMSE. Fine-tuning the model for specific stations in Corsica further improves forecasting accuracy, particularly for smallest time horizons. This approach that leverages the optimal weights obtained from the global training phase mitigates overfitting when one wants to adapt the model to a specific location.

In the context of extreme wind prediction, defined as the occurrence of wind speeds exceeding high quantiles (e.g., 90%, 95%, 99%) of site-specific distributions, we demonstrate that the probabilistic model significantly outperforms linear regression models and post-processed AROME predictions, especially at longest forecasting horizons. We also show that our approach yields much more accurate predictions compared to its deterministic counterpart, which is based solely on the expected mean value. Moreover, the model's performance improves as the quantile increases. This observation will have to be further investigated using a larger dataset, as it suggests that, in terms of PSS score, conditions leading to very strong wind events may be easier to anticipate than those associated with milder wind speeds.

In conclusion, the hybrid neural network model demonstrates significant improvements in short-term wind speed forecasting by integrating NWP data with ground station observations. Its ability to provide both deterministic and probabilistic forecasts makes it a valuable tool for applications in renewable energy, public safety, and operational decision-making. A perspective for future work is focusing on the probabilistic aspects of the model to improve its reliability in terms of probabilistic metrics as logScore or CRPS (Baggio and Muzy 2024). Our parametric approach can be directly compared with the non-parametric model based on normalizing flows proposed by (Marcille et al. 2024). Additionally, our predictions could be improved by leveraging, as pioneered by Rasp and Lerch (2018), ensemble NWP forecasting. This can potentially leads to better

risk assessment for extreme events (Primo et al. 2024). Another promising direction involves incorporating additional data sources such as orography or surface roughness, that have been demonstrated to influence the reliability of wind speed predictions (Rasp and Lerch 2018; Veldkamp et al. 2021). Finally, advancements in deep learning architectures offer appealing opportunities for further refinement. While LSTMs and CNNs have demonstrated strong performance, recent advances in Transformer-based models have shown great potential for capturing long-range dependencies in spatiotemporal data (see, e.g., Ødegaard Bentsen et al. (2023)).

*Acknowledgments.* This work was partially supported by ANR grant SAPHIR project ANR-21-CE04-001403.

*Data availability statement.* This work uses the MeteoNet open reference dataset by Meteo France (Larvor et al. 2020).

## APPENDIX

### The M-Rice distribution

The Rice distribution corresponds to the amplitude (i.e. the norm) of a two dimensional random vector which components are 2 independent Gaussian random variables of same variance. It has been extended in Baïle et al. (2011) to M-Rice that account for the situation when, as observed in turbulence models, this variance is itself stochastic with a log-normal distribution. The density for a M-Rice distribution involves 3 parameters, namely the two Rice parameters coming from from Gaussian law  $\nu$  and  $\sigma^2$  and a supplementary parameter, denoted as  $\lambda^2$  associated with the variance of the log-normal law. Its density reads:

$$\begin{aligned} f_{MR}(y|\nu, \sigma, \lambda^2) &= \frac{1}{\sqrt{2\pi\lambda^2}} \int e^{-\frac{\omega^2}{2\lambda^2}} f_R(y, \nu, \sigma e^\omega) d\omega \\ &= \frac{1}{\sqrt{2\pi\lambda^2}} \int e^{-\frac{\omega^2}{2\lambda^2}} \frac{y}{e^{2\omega\sigma^2}} e^{-\frac{y^2 + \nu^2}{2e^{2\omega}\sigma^2}} I_0\left(\frac{y\nu}{e^{2\omega}\sigma^2}\right) d\omega \end{aligned}$$

where the parameter  $\lambda^2$  is referred to, in the literature on turbulence, as the ‘‘intermittency coefficient’’ Frisch (1995). As advocated in Baggio and Muzy (2024), this last formula is evaluated using the following Gauss-Hermite quadrature:

$$\int_{-\infty}^{+\infty} e^{-y^2} f(y) dy \approx \sum_{i=1}^n w_i f(y_i) \quad (\text{A1})$$

were  $n \geq 1$ , the abscissa  $\{y_i\}_{i=1, \dots, n}$  correspond to the roots of the order  $n$ -th Hermite polynomial  $H_n(y)$  and the weights  $\{w_i\}_{i=1, \dots, n}$  are:

$$w_i = \frac{2^{n-1} n! \sqrt{\pi}}{n^2 [H_{n-1}(y_i)]^2}$$

with  $n = 11$  that is sufficient for the purpose of this paper (Baggio and Muzy 2024).

Since for a Rice law of parameter  $\nu$  and  $\sigma^2$ , the mean value is  $\mu_1 = \sigma \sqrt{\frac{\pi}{2}} L_{\frac{1}{2}} \left( -\frac{\nu^2}{2\sigma^2} \right)$ , where  $L_{\frac{1}{2}}$  stands for the order  $\frac{1}{2}$  Laguerre polynomial, the mean value of a M-Rice distribution reads:

$$\begin{aligned} \mu_R(\nu, \sigma, \lambda^2) &= \frac{\sigma}{\sqrt{2}} \int e^{-y^2} L_{\frac{1}{2}} \left( -\frac{e^{2\sqrt{2}\lambda y} \nu^2}{2\sigma^2} \right) dy \\ &\simeq \frac{\sigma}{\sqrt{2}} \sum_{i=1}^n w_i L_{\frac{1}{2}} \left( -\frac{e^{2\sqrt{2}\lambda y_i} \nu^2}{2\sigma^2} \right) \quad (\text{A2}) \end{aligned}$$

## References

- Baggio, R., and J.-F. Muzy, 2024: Improving probabilistic wind speed forecasting using m-rice distribution and spatial data integration. *Applied Energy*, **360**, 122 840, <https://doi.org/https://doi.org/10.1016/j.apenergy.2024.122840>.
- Baïle, R., J. F. Muzy, and P. Poggi, 2011: An M-Rice wind speed frequency distribution. *Wind Energy*, **14**, 735–748.
- Bauer, P., A. Thorpe, and G. Brunet, 2015: The quiet revolution of numerical weather prediction. *Nature*, **525** (7567), 47–55, <https://doi.org/10.1038/nature14956>.
- Baïle, R., and J.-F. Muzy, 2023: Leveraging data from nearby stations to improve short-term wind speed forecasts. *Energy*, **263**, 125 644, <https://doi.org/https://doi.org/10.1016/j.energy.2022.125644>.
- Baïle, R., J. F. Muzy, and P. Poggi, 2011: Short-term forecasting of surface layer wind speed using a continuous random cascade model. *Wind Energy*, **14** (6), 719–734, <https://doi.org/10.1002/we.452>, <https://onlinelibrary.wiley.com/doi/pdf/10.1002/we.452>.
- Brabec, M., A. Craciun, and A. Dumitrescu, 2021: Hybrid numerical models for wind speed forecasting. *Journal of Atmospheric and Solar-Terrestrial Physics*, **220**, 105 669, <https://doi.org/https://doi.org/10.1016/j.jastp.2021.105669>.
- Breiman, L., 2001: Random forests. *Machine Learning*, **45**, 5–32, <https://doi.org/10.1023/A:1010933404324>.
- Coquillat, S., and Coauthors, 2019: SAETTA: high-resolution 3-D mapping of the total lightning activity in the Mediterranean Basin over Corsica, with a focus on a mesoscale convective system event. *Atmospheric Measurement Techniques*, **12** (11), 5765–5790, <https://doi.org/10.5194/amt-12-5765-2019>.
- Courtier, P., J.-N. Thépaut, and A. Hollingsworth, 1994: A strategy for operational implementation of 4D-Var, using an incremental approach. *Quart. J. Roy. Meteor. Soc.*, **120** (519), 1367–1387, <https://doi.org/10.1002/qj.49712051912>.
- Donadio, L., J. Fang, and F. Porté-Agel, 2021: Numerical weather prediction and artificial neural network coupling for wind energy forecast. *Energies*, **14** (2), <https://doi.org/10.3390/en14020338>.
- Drobinski, P., and Coauthors, 2014: HyMeX: A 10-Year Multi-disciplinary Program on the Mediterranean Water Cycle. *Bull. Amer. Meteor. Soc.*, **95** (7), 1063–1082, <https://doi.org/10.1175/BAMS-D-12-00242.1>.
- Frisch, U., 1995: *Turbulence*. Cambridge Univ. Press, Cambridge.
- Gneiting, T., A. E. Raftery, A. H. Westveld, and T. Goldman, 2005: Calibrated probabilistic forecasting using ensemble model output statistics and minimum crps estimation. *Mon. Wea. Rev.*, **133** (5), 1098–1118, <https://doi.org/10.1175/MWR2904.1>.
- Goodfellow, I., Y. Bengio, and A. Courville, 2016: *Deep learning*. MIT Press, Cambridge, MA.
- Hanifi, S., X. Liu, Z. Lin, and S. Lotfian, 2020: A critical review of wind power forecasting methods—past, present and future. *Energies*, **13** (15), <https://doi.org/10.3390/en13153764>.
- Hatzaki, M., and Coauthors, 2023: MedCyclones: Working Together toward Understanding Mediterranean Cyclones. *Bull. Amer. Meteor. Soc.*, **104** (2), E480–E487, <https://doi.org/10.1175/BAMS-D-22-0280.1>.
- He, B., L. Ye, M. Pei, P. Lu, B. Dai, Z. Li, and K. Wang, 2022: A combined model for short-term wind power forecasting based on the analysis of numerical weather prediction data. *Energy Reports*, **8**, 929–939, <https://doi.org/https://doi.org/10.1016/j.egy.2021.10.102>.
- Hoolohan, V., A. S. Tomlin, and T. Cockerill, 2018: Improved near surface wind speed predictions using gaussian process regression combined with numerical weather predictions and observed meteorological data. *Renewable Energy*, **126**, 1043–1054, [https://doi.org/10.1016/j.renene.2018.04.019](https://doi.org/https://doi.org/10.1016/j.renene.2018.04.019).
- Huang, L., G. Isaac, and G. Sheng, 2012: Integrating nwp forecasts and observation data to improve nowcasting accuracy. *Wea. Forecasting*, **27**, 938–953, <https://doi.org/10.1175/WAF-D-11-00125.1>.
- Jolliffe, I. T., Ed., 2004: *Forecast verification: a practitioner's guide in atmospheric science*. repr ed., Wiley, Chichester.
- Klawe, M., and U. Ulbrich, 2003: A model for the estimation of storm losses and the identification of severe winter storms in Germany. *Natural Hazards and Earth System Sciences*, **3** (6), 725–732, <https://doi.org/10.5194/nhess-3-725-2003>.
- Larvor, G., L. Berthomier, V. Chabot, B. L. Pape, B. Pradel, and L. Perez, 2020: MeteoNet: an open reference dataset by METEO FRANCE. URL <https://github.com/meteofrance/meteonet/>, GitHub repository.
- Lfarh, W., F. Pantillon, and J.-P. Chaboureau, 2023: The Downward Transport of Strong Wind by Convective Rolls in a Mediterranean Windstorm. *Mon. Wea. Rev.*, **151** (10), 2801–2817, <https://doi.org/10.1175/MWR-D-23-0099.1>.
- Marcille, R., P. Tandeo, M. Thiébaud, P. Pinson, and R. Fablet, 2024: Convolutional encoding and normalizing flows: A deep learning approach for offshore wind speed probabilistic forecasting in the mediterranean sea. *Artificial Intelligence for the Earth Systems*, **3** (3), 230 112, <https://doi.org/10.1175/AIES-D-23-0112.1>.
- Mason, I., 1979: On reducing probability forecasts to yes/no forecasts. *Mon. Wea. Rev.*, **107** (2), 207–211, [https://doi.org/10.1175/1520-0493\(1979\)107<0207:ORPFTY>2.0.CO;2](https://doi.org/10.1175/1520-0493(1979)107<0207:ORPFTY>2.0.CO;2).
- Pantillon, F., B. Adler, U. Corsmeier, P. Knippertz, A. Wieser, and A. Hansen, 2020: Formation of Wind Gusts in an Extratropical Cyclone in Light of Doppler Lidar Observations and Large-Eddy Simulations. *Mon. Wea. Rev.*, **148** (1), 353–375, <https://doi.org/10.1175/MWR-D-19-0241.1>.

- Pantillon, F., S. Lerch, P. Knippertz, and U. Corsmeier, 2018: Forecasting wind gusts in winter storms using a calibrated convection-permitting ensemble. *Quart. J. Roy. Meteor. Soc.*, **144** (715), 1864–1881, <https://doi.org/10.1002/qj.3380>.
- Pelosi, A., H. Medina, J. V. den Bergh, S. Vannitsem, and G. B. Chirico, 2017: Adaptive kalman filtering for postprocessing ensemble numerical weather predictions. *Mon. Wea. Rev.*, **145** (12), 4837 – 4854, <https://doi.org/10.1175/MWR-D-17-0084.1>.
- Pinto, J. G., F. Pantillon, P. Ludwig, M.-S. Déroche, G. Leoncini, C. C. Raible, L. C. Shaffrey, and D. B. Stephenson, 2019: From Atmospheric Dynamics to Insurance Losses – an Interdisciplinary Workshop on European Storms. *Bull. Amer. Meteor. Soc.*, BAMS–D–19–0026.1, <https://doi.org/10.1175/BAMS-D-19-0026.1>.
- Primo, C., B. Schulz, S. Lerch, and R. Hess, 2024: Comparison of model output statistics and neural networks to postprocess wind gusts. URL <https://arxiv.org/abs/2401.11896>, 2401.11896.
- Quinn, J., J. McEachen, M. Fullan, M. Gardner, and M. Drummy, 2019: *Dive Into Deep Learning: Tools for Engagement*. SAGE Publications, URL <https://books.google.fr/books?id=o55LxAEACAAJ>.
- Rasp, S., and S. Lerch, 2018: Neural Networks for Postprocessing Ensemble Weather Forecasts. *Mon. Wea. Rev.*, **146** (11), 3885–3900, <https://doi.org/10.1175/MWR-D-18-0187.1>.
- Salinas, D., V. Flunkert, J. Gasthaus, and T. Januschowski, 2020: DeepAR: Probabilistic forecasting with autoregressive recurrent networks. *International Journal of Forecasting*, **36** (3), 1181–1191, <https://doi.org/10.1016/j.ijforecast.2019.07.001>.
- Scheffknecht, P., E. Richard, and D. Lambert, 2017: Climatology of heavy precipitation over Corsica in the period 1985–2015. *Quart. J. Roy. Meteor. Soc.*, **143** (709), 2987–2998, <https://doi.org/10.1002/qj.3140>.
- Seity, Y., P. Brousseau, S. Malardel, G. Hello, P. Bénard, F. Bouttier, C. Lac, and V. Masson, 2011: The AROME-France Convective-Scale Operational Model. *Mon. Wea. Rev.*, **139** (3), 976–991, <https://doi.org/10.1175/2010MWR3425.1>.
- Shaw, W. J., and Coauthors, 2019: The Second Wind Forecast Improvement Project (WFIP2): General Overview. *Bull. Amer. Meteor. Soc.*, **100** (9), 1687–1699, <https://doi.org/10.1175/BAMS-D-18-0036.1>.
- Swinbank, R., and Coauthors, 2016: The TIGGE Project and Its Achievements. *Bull. Amer. Meteor. Soc.*, **97** (1), 49–67, <https://doi.org/10.1175/BAMS-D-13-00191.1>.
- Tascikaraoglu, A., and M. Uzunoglu, 2014: A review of combined approaches for prediction of short-term wind speed and power. *Renewable and Sustainable Energy Reviews*, **34**, 243–254, <https://doi.org/https://doi.org/10.1016/j.rser.2014.03.033>.
- Vannitsem, S., and Coauthors, 2021: Statistical Postprocessing for Weather Forecasts: Review, Challenges, and Avenues in a Big Data World. *Bull. Amer. Meteor. Soc.*, **102** (3), E681–E699, <https://doi.org/10.1175/BAMS-D-19-0308.1>.
- Veldkamp, S., K. Whan, S. Dirksen, and M. Schmeits, 2021: Statistical postprocessing of wind speed forecasts using convolutional neural networks. *Mon. Wea. Rev.*, **149** (4), 1141 – 1152, <https://doi.org/10.1175/MWR-D-20-0219.1>.
- Wang, Y., R. Zou, F. Liu, L. Zhang, and Q. Liu, 2021: A review of wind speed and wind power forecasting with deep neural networks. *Applied Energy*, **304**, 117766, <https://doi.org/https://doi.org/10.1016/j.apenergy.2021.117766>.
- Wilks, D. S., 2019: Chapter 9 - forecast verification. *Statistical Methods in the Atmospheric Sciences (Fourth Edition)*, D. S. Wilks, Ed., fourth edition ed., Elsevier, 369–483, <https://doi.org/10.1016/B978-0-12-815823-4.00009-2>.
- Yano, J.-I., and Coauthors, 2018: Scientific Challenges of Convective-Scale Numerical Weather Prediction. *Bull. Amer. Meteor. Soc.*, **99** (4), 699–710, <https://doi.org/10.1175/BAMS-D-17-0125.1>.
- Zamo, M., L. Bel, O. Mestre, and J. Stein, 2016: Improved gridded wind speed forecasts by statistical postprocessing of numerical models with block regression. *Wea. Forecasting*, **31** (6), 1929 – 1945, <https://doi.org/10.1175/WAF-D-16-0052.1>.
- Ødegaard Bentsen, L., N. D. Warakagoda, R. Stenbro, and P. Engelstad, 2023: Spatio-temporal wind speed forecasting using graph networks and novel transformer architectures. *Applied Energy*, **333**, 120565, <https://doi.org/10.1016/j.apenergy.2022.120565>.